Supplementary Information (SI) for Materials Horizons.
This journal is © The Royal Society of Chemistry 2024

Supporting Information

Comb-like poly(β-amino ester)-integrated PEO-based self-healing solid electrolyte with fast ion conduction for lithium–sulfur batteries

Hui-Min Wang[a,b], Mengdi Geng[a], Jing Bai[a], Dezhong Zhou[*c], Weibo Hua[c], Sheng Liu[*a] and Xueping Gao[*a]

a. Institute of New Energy Material Chemistry, School of Materials Science and Engineering, Nankai University, Tianjin 300350, China. *Email: shengliu@nankai.edu.cn, xpgao@nankai.edu.cn

b. School of Materials Science and Engineering, Sichuan University of Science & Engineering, Sichuan, Zigong 643000, China.

c. School of Chemical Engineering and Technology, Xi'an Jiaotong University, Xi'an 710049, China. *Email: dezhong.zhou@xjtu.edu.cn

Experimental Section

Preparation of PAE and PPAEs

Firstly, PEGDA, [4-(aminomethyl)phenyl] boronic acid and triethylamine were dissolved in anhydrous dimethyl sulfoxide (DMSO) with a molar ratio of 1:1:1.3, and the monomer concentration was 500 mg mL^{-1}. The reaction proceeds at 120 °C under magnetic stirring. After 3 hours, the reaction was stopped by cooling down to room temperature (RT) as the M_w was approached 40 kDa. Subsequently, PEGDA was further added and diluted with DMSO to a final concentration of 100 mg mL^{-1} to end-cap the polymer at 25 °C for 48 hours. After purifying the resulting polymers with three diethyl ether washes and drying in a vacuum chamber at RT, PAE was obtained.

PEO (M_w = 600,000), lithium bis(trifluoromethanesulphony)imide (LiTFSI) (EO:Li = 18:1, molar ratio) and different contents of PAE (2%, 6%, 10% relative to PEO) were mixed in 1-Methyl-2-pyrrolidinone (NMP) and stirred for 12 hours. Then, 1 wt% 2-hydroxy-2-methyl-1-phenyl-1-propanone (HMPP) as a light initiator was added to the mixture. After stirring uniformly, the solution was poured onto a Teflon membrane and irradiated under UV light (λ = 365 nm) for 20 minutes, then dried at 80 °C for 48 hours and punched into 16 mm disks. For comparison, the PEO-SPE was prepared similarly by casting the PEO/LiTFSI solution onto a Teflon membrane and drying it in vacuum oven at 80 °C for 48 hours.

Material characterization

The M_w of polymers were determined using GPC (Agilent 1260 infinity II). The chemical compositions and structures of polymers were confirmed by ^1H nuclear magnetic resonance (NMR, JNM-ECZ400S/L1) and Fourier transform infrared (FTIR, Bruker-TENSOR 37). The morphologies and elemental distribution spectroscopy (EDS) mappings of SPE were analysed using field emission scanning electron microscopy (SEM, JSM−7800F). The crystallographic structure of SPEs was studied by X-ray diffraction spectrum (XRD, Rigaku mini Flex II). The

differential scanning calorimetry (DSC) analysis was measured with METTLER TOLEDO, TGA/DSC1, and the stress-strain test was performed on a universal tensile testing machine (SHIMADZU TRAPEZIUMX, Japan). The composition of the SEI was analyzed by the X-ray photoelectron spectra (XPS, PHI5000 Versa Probe-ESCALAB 250xi). Raman spectra were recorded by the Raman spectrometer (TEO SR-500I-A). Solid-state ^{1}H and ^{7}Li NMR measurements were performed on Bruker Avance III WB 400 spectrometer.

Preparation of the cathode electrode

Firstly, sulfur and carbon nanotubes were blended at a weight ratio of 7:3 and then heated to 155 °C for 12 hours to obtain the S/C composite. Next, the S/C composite, super P, binder of PEO and LiTFSI (EO:Li = 18:1, molar ratio) with a mass ratio of 6:1:3 were dispersed in NMP. The obtained slurry was then coated on the current collector of Al foil and dried at 60 °C. Then it was cut into 10 mm disks. The active material loading of sulfur was 0.6–0.8 mg cm^{-2}. Composite cathode electrodes with higher S-content (49%) and S-loading (1.0 and 4.3 mg cm^{-2}) were prepared with the S/C composite, super P, binder of PEO and LiTFSI (EO:Li = 18:1, molar ratio) with a mass ratio of 7:1:2.

Electrochemical measurement

Electrochemical impedance spectroscopy (EIS) tests were conducted using SS │ SPE │ SS symmetric cells on an electrochemical workstation (Zahner IM6ex) from 20 to 60 °C, with the frequency range from 100 mHz to 1 MHz, and the amplitude voltage was 10 mV. The ionic conductivity of SPE was calculated as the equation of $\sigma = L/(SR)$, where L, S, and R were the SPE thickness (cm), SPE area (cm^2), and SPE resistance (Ω), respectively. The t_{Li^+} was measured in Li │ SPE │ Li symmetric cell with DC polarization at 60°C, which was calculated as: $t_{Li^+} = I_S(\Delta V - I_0R_0)/I_0(\Delta V - I_SR_S)$. I_S, I_0 stand for the steady-state and initial currents, R_S, R_0 present the steady-state and initial resistances, ΔV was 10 mV. The linear sweep voltammetry (LSV) and cyclic voltammetry (CV) curves were tested by the CHI 600A electrochemical workstation with a scan rate of 0.5 mV s^{-1} and 0.1 mV s^{-1}, respectively. The discharge/charge

tests were performed in Li │ SPE │ S/C CR2032 coin cells at a voltage range of 1.6–2.8 V using the LAND test system (LAND CT2001A). All the electrochemical measurements were conducted at 60 °C.

Supplementary Figures

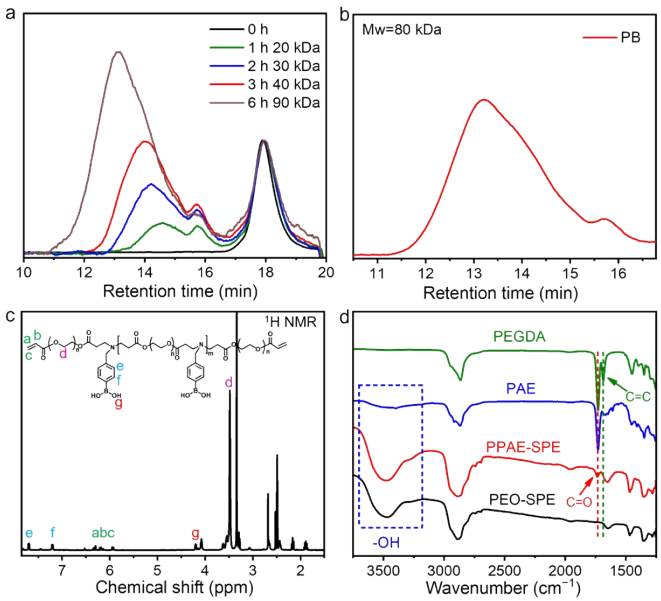

Figure S1. (a) The molecular weight evolution of PAE monitored by GPC. (b) GPC spectrum of purified PAE. (c) ^{1}H NMR spectrum of PAE. (d) FTIR spectra of PEGDA, PAE, PPAE-SPE, and PEO-SPE.

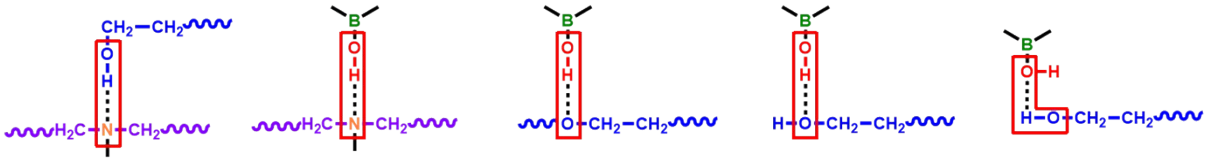

Figure S2. The quintuple hydrogen bonds in PPAE-SPE.

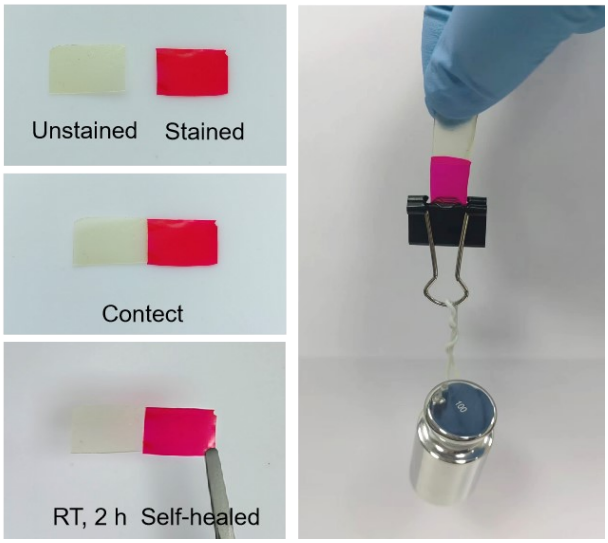

Figure S3. Self-healing tests of PPAE-SPE.

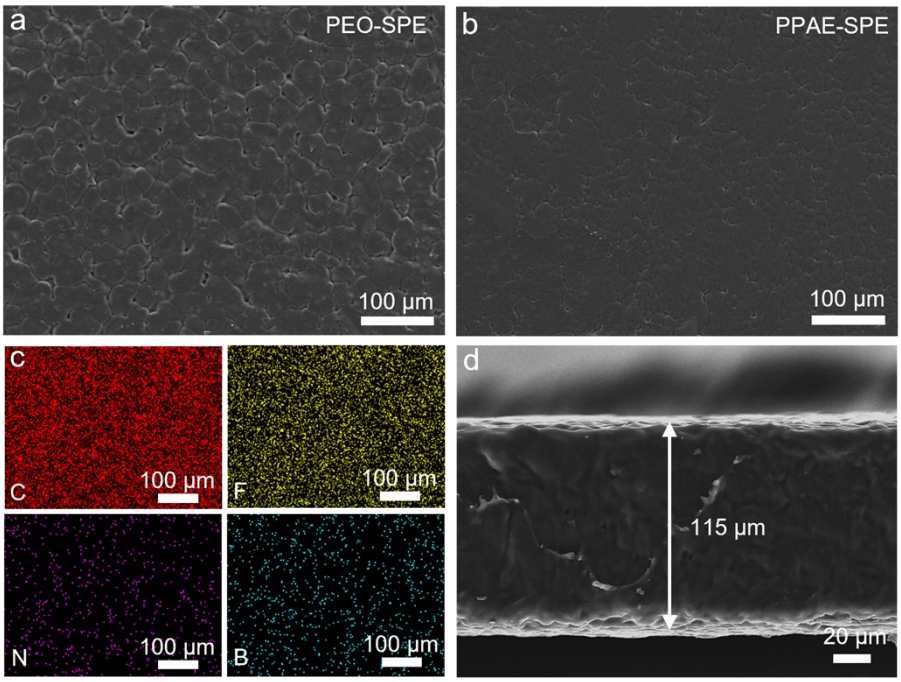

Figure S4. SEM images of (a) PEO-SPE and (b) PPAE-SPE. (c) EDS mappings and (d) cross-sectional SEM images of PPAE-SPE.

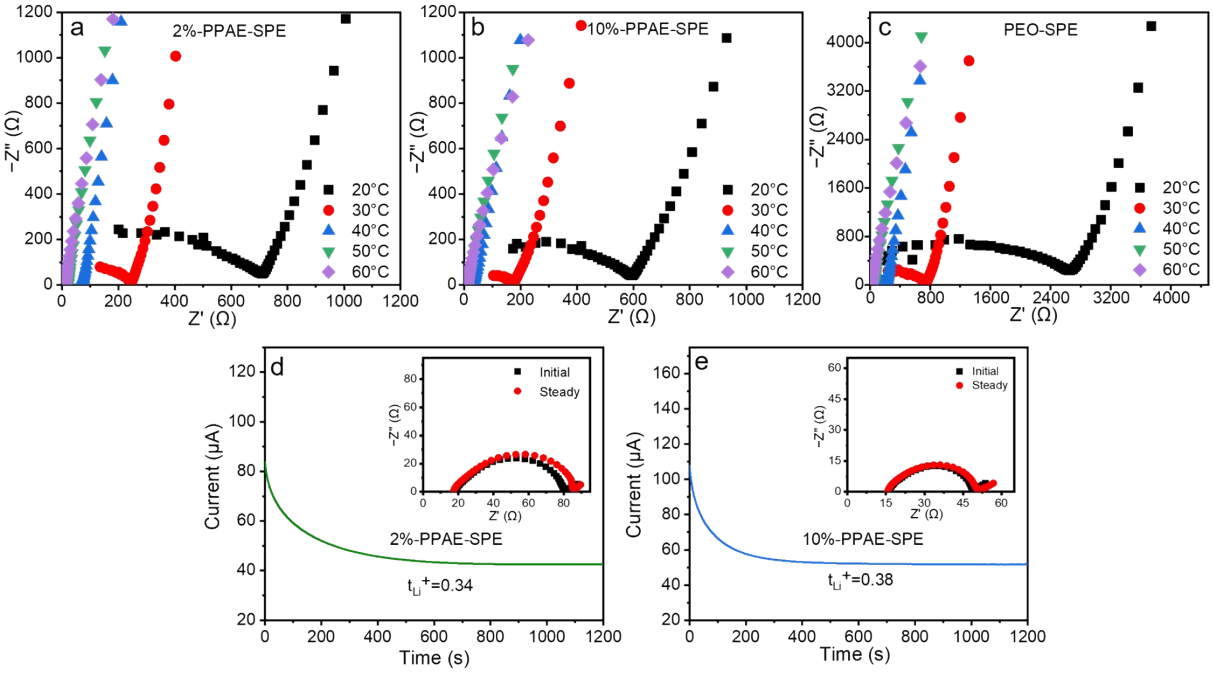

Figure S5. (a-c) EIS plots of PPAE-SPEs from 20 to 60 °C. (d, e) Lithium-ion transference numbers 2%-PPAE-SPE and 10%-PPAE-SPE.

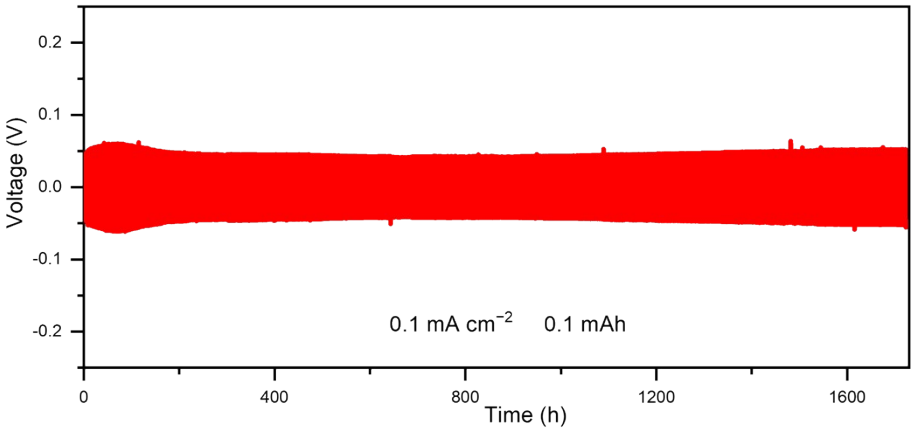

Figure S6. The voltage profile of lithium symmetrical cell with PPAE-SPE at 0.1 mA cm^{-2}.

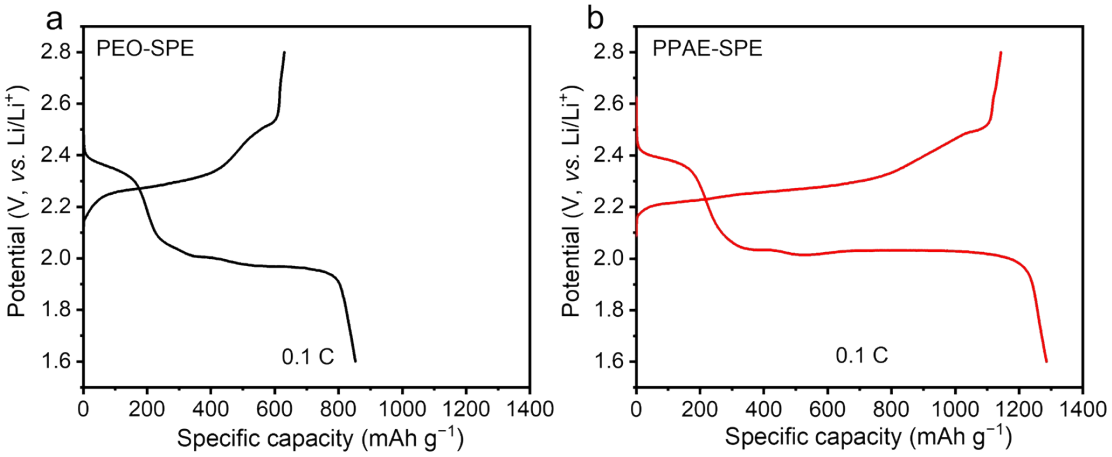

Figure S7. The initial discharge/charge curves of the cells with (a) PEO-SPE and (b) PPAE-SPE at 0.1 C.

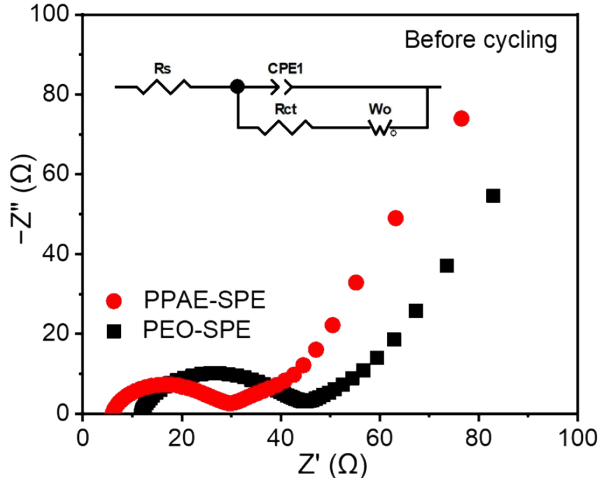

Figure S8. EIS plots of the cells with PEO-SPE and PPAE-SPE before cycling.

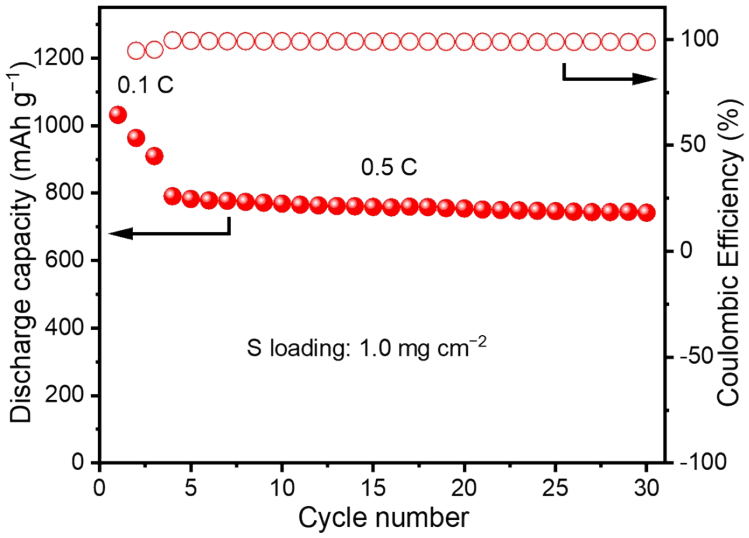

Figure S9. Cycling performance of the cells with PPAE-SPE at 0.5 C.

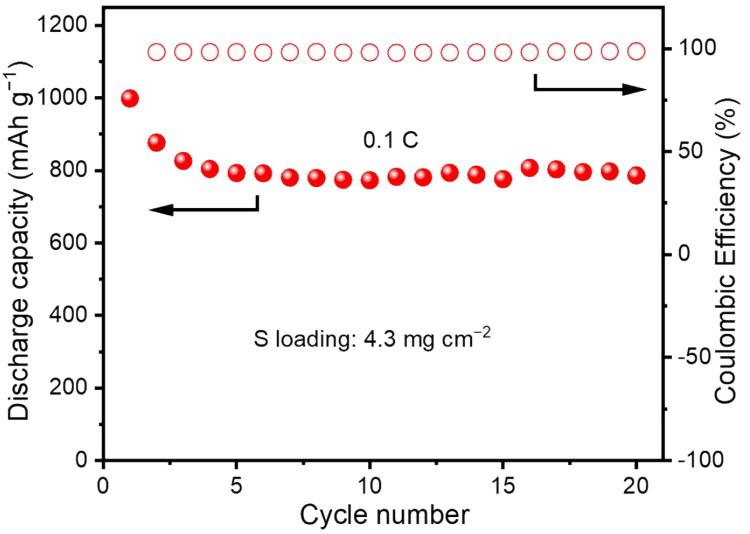

Figure S10. Cycling performance of the cells using PPAE-SPE with heavy S-loading.

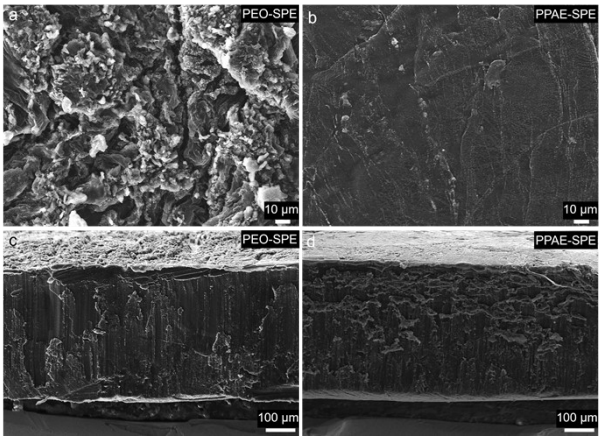

Figure S11. SEM images of the Li anodes retrieved from the Li–S cells with PEO-SPE and PPAE-SPE after 80 cycles. (a, b) Surface morphology and (c, d) cross-sectional morphology.

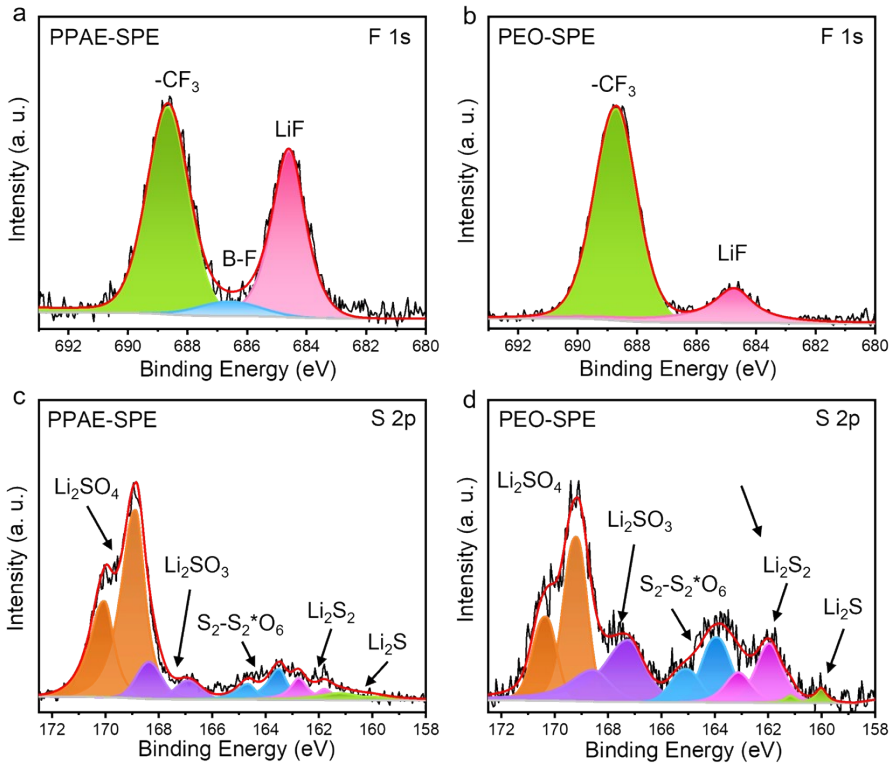

Figure S12. XPS analysis for F 1s and S 2p of the Li anodes retrieved from the Li–S cells with (a, c) PPAE-SPE and (b, d) PEO-SPE.

Supplementary Tables

Table S1. Ionic conductivity of PEO-SPE and PPAE-SPE at different temperatures.

Electrolytes	σ (S cm^{-1})				
	20 ℃	30 ℃	40 ℃	50 ℃	60 ℃
PEO-SPE	1.88×10^{-6}	7.66×10^{-6}	2.37×10^{-5}	9.90×10^{-5}	3.14×10^{-4}
PPAE-SPE	1.25×10^{-5}	4.20×10^{-5}	2.21×10^{-4}	4.63×10^{-4}	6.48×10^{-4}

Table S2. Summary of ionic conductivity of different SPEs.

Electrolyte composition	σ (S cm^{-1})				Ref.
	30 ℃	40 ℃	50 ℃	60 ℃	
PI/PEO/LiTFSI	3.68×10^{-5}	—	—	1.54×10^{-4}	S1
PEO/LLZTO/LiTFSI/acetamide/LiDFOB				5.10×10^{-5}	S2
PEO/LiTFSI/In_2O_3	—	—	—	5.27×10^{-4}	S3
PEO/LiTFSI/6% h-BN	7.70×10^{-6}	1.91×10^{-5}	4.70×10^{-5}	8.90×10^{-5}	S4
PEO/PI/LiPFSI				2.70×10^{-4}	S5
PEO/LiTFSI/Al_2O_3–δ-600	—	—	—	3.81×10^{-4}	S6
21-β-CD-g-PTFEMA /PEO/ LiTFSI	6.57×10^{-6}	2.45×10^{-5}	1.43×10^{-4}	3.20×10^{-4}	S7
PPAE-SPE	4.20×10^{-5}	2.21×10^{-4}	4.63×10^{-4}	6.48×10^{-4}	**This work**

Table S3. Summary of electrochemical properties of different SPEs

Electrolyte composition	Li symmetrical cells	Li–S cells			Ref.
	Current density (mA cm^{-2})/Life (h)	S loading (mg cm^{-2})	Initial capacity (mAh g^{-1})/C rate	Temperature (℃)	
PEO/LiTFSI/TMPETA/PEGDMA	0.1/1600	0.8	1133/0.1 C	60	42
PEO/LLZTO/LiTFSI/acetamide/LiDFOB	0.1/1000	0.7-0.9	1012/0.05 C	60	S2
AQT@PEO/LiTFSI	—	0.2-0.7	1133/0.1 C	60	S8
PEO/LiTFSI//LiBAMB/PETMA/DMPA	0.25/350	0.8	1040/0.1 C	80	S9
PEO/LiTFSI/PFA	0.1/500	0.5	1170/0.05 mA cm^{-2}	60	S10
PEO-LLZTO-MgF_2	0.2/500	0.5	812/0.2 C	60	S11
PPAE-SPE	0.2/800	0.6-0.8	826.1/0.2 C 1285.8/0.1 C	60	**This work**

Reference:

[S1] J. Wu, Z. Rao, Z. Cheng, L. Yuan, Z. Li and Y. Huang, Advanced Energy Materials, 2019, **9**, 1902767.

[S2] M. Li, Z. Huang, Y. Liang, Z. Wu, H. Zhang, H. Chen and S. Zhang, Advanced Functional Materials, 2024, 2413580.

[S3] X. Zhang, H. Zhang, Y. Geng, Z. Shi, S. Zhu, Q. Xu, Y. Min, Chemical Engineering Journal, 2022, **444**, 136328.

[S4] Y. Li, L. Zhang, Z. Sun, G. Gao, S. Lu, M. Zhu, Y. Zhang, Z. Jia, C. Xiao, H. Bu, K. Xi and S. Ding, Journal of Materials Chemistry A, 2020, **8**, 9579–9589.

[S5] J. Li, H. Hu, W. Fang, J. Ding, D. Yuan, S. Luo, H. Zhang and X. Ji, Advanced Functional Materials, 2023, **33**, 2303718.

[S6] Y. Song, L. Yang, J. Li, M. Zhang, Y. Wang, S. Li, S. Chen, K. Yang, K. Xu and F. Pan, Small, 2021, **17**, 2102039.

[S7] Y. Su, X. Rong, A. Gao, Y. Liu, J. Li, M. Mao, X. Qi, G. Chai, Q. Zhang, L. Suo, L. Gu, H. Li, X. Huang, L. Chen, B. Liu, Y.-S. Hu, Nature Communications, 2022, **13**, 4181.

[S8] X. Gao, X. Zheng, Y. Tsao, P. Zhang, X. Xiao, Y. Ye, J. Li, Y. Yang, R. Xu, Z. Bao and Y. Cui, Journal of the American Chemical Society, 2021, **143**, 43, 18188–18195.

[S9] L. Zhong, S. Wang, M. Xiao, W. Liu, D. Han, Z. Li, J. Qin, Y. Li, S. Zhang, S. Huang, Y. Meng, Energy Storage Materials, 2021, **41**, 563–570.

[S10] Y. An, Y. Cheng, S. Wang and J. Yu, ACS Applied Energy Materials, 2022, **5**, 2786−2794.

[S11] H. Duan, L. Liao, R. Bi, Y. Deng and G. Chen, Journal of Materials Chemistry A, 2023, **11**, 19046–19055.